WILEY | The International Journal of **Medical Robotics** and **Computer Assisted Surgery**

ORIGINAL ARTICLE

Fine orientation control of an insertable robotic camera system for single incision laparoscopic surgery

Reza Yazdanpanah Abdolmalaki[1] | Xiaolong Liu[1] | Gregory J. Mancini[2] | Jindong Tan[1]

[1]Department of Mechanical, Aerospace, and Biomedical Engineering, University of Tennessee, Knoxville, Tennessee,
[2]Graduate School of Medicine, University of Tennessee, Knoxville, Tennessee,

Correspondence
Xiaolong Liu, Department of Mechanical, Aerospace and Biomedical Engineering, University of Tennessee, Knoxville, TN 37996.
Email: xliu57@vols.utk.edu

Abstract

Background: Insertable laparoscopic camera systems were developed to improve the minimally invasive surgeries. Robotic degrees of freedom for an insertable laparoscopic camera are required to adjust the camera's orientation and position inside an abdominal cavity.

Methods: This paper demonstrates an insertable magnetic actuated robotic camera system with two-degree-of-freedom (2-DoF) orientation control for single incision laparoscopic surgery. The camera system design consists of an external magnetic control unit and a fully insertable camera capsule. This system features a unified mechanism for anchoring, navigating, and rotating the insertable camera capsule by externally generated rotational magnetic field from the control unit. The motor-free camera capsule is encapsulated in an one-piece housing with two ring-shaped tail-end magnets and one cylindrical central magnet. The control unit that positioned externally consists of both permanent magnets and electromagnetic coils to generate rotational magnetic field and control the camera capsule.

Results: The experimental investigations indicated that the camera control system can achieve less than 1° control accuracies with average errors 0.594° and 0.524° for tilt motion and pan motion, respectively.

Conclusion: The designed control system provides fine orientation control for the insertable camera capsule which guarantees proper vision for the surgeon during single incision laparoscopic surgery.

KEYWORDS
laparoscopic surgery, magnetic actuation, robotic camera system

1 | INTRODUCTION

Minimally invasive surgery (MIS) has been widely applied to achieve less operative bleeding and postoperative pain, faster recovery time, and better cosmetic results.[1,2] This surgical procedure requires making small incisions on patient anatomy to insert surgical instruments, which are manipulated inside the patient's body. Since the line-of-sight between surgeon eyes and surgical instruments is occluded by the patient's abdominal wall, a long-stick laparoscopic camera for visual feedback can be applied through a dedicated incision or a shared incision with other surgical instruments. To improve triangulation and manipulating flexibility between a long-stick camera and other surgical instruments, insertable laparoscopic cameras were developed.[3,4]

Robotic degrees of freedom (DoFs) for an insertable laparoscopic camera are required to adjust the camera's orientation and position inside an abdominal cavity. The cameras need to be mounted on the internal surface of an insufflated abdominal wall. Some camera designs are mounted on abdominal walls by suturing/piercing/magnetic fixation and controlled by on-board motors with peripheral mechanisms for 2-DoF rotation.[5-7] To reduce the design complexity and decrease the camera size, it is preferred to reduce the usages of on-board motors. The cameras' robotic DoFs, such as 2-DoF navigation and 1-DoF rotation (pan motion), can be activated by the magnetic coupling between external magnetic handle and internal magnets.[8-10] To control the rest 1-DoF for tilt motion in those camera designs, on-board motors are still required.

Efforts have been made on eliminating on-board motors to simplify the actuation mechanism and to reduce power consumption, especially for a wireless laparoscopic camera. Manual manipulation between external magnetic handle and internal magnet can actuate 1-DoF rotation.[11] Automatic control of 2-DoF rotational motion for an insertable camera can be achieved by using electromagnetic coils to drive internal magnet array[12] or using one motorized external magnet to drive orthogonally arranged internal magnets.[13] Both of the

two designs work well for close proximity, such as 20-mm abdominal wall thickness. Considering the normal range of abdominal wall thickness, ie, 20 to 40 mm,[14] the control stability and reliability will be significantly reduced as an abdominal wall thickness increases.

Insertable laparoscopic camera system potentially improves the MIS in multiple aspects: (1) In traditional MIS, it reduces an incision that is specified for insertion of long-stick laparoscopic camera; (2) in single incision laparoscopic surgeries (SILS), it reduces the port complexity and enhances dexterity of other surgical instruments consequently; (3) mobile camera systems offer proper and wider view angle of surgical site without imposing limitations for other instruments; and (4) an insertable camera system provides proper foundation for implementation of additional systems to improve surgical imaging features such as enhanced surgical illumination[15] and *in vivo* lens cleaning mechanism.[16]

In our prior work,[17] we designed a reliable magnetic actuation mechanism for insertable laparoscopic cameras, which enables two rotational DoFs under normal range of abdominal wall thickness. The design consists of an external hybrid magnetic driving unit and an internal driven unit. The hybrid magnetic driving unit adopts three permanent magnets and two electromagnetic coils, which are orthogonally arranged as shown in Figure 1. Rotational magnetic field, which actuates the 2-DoF rotational motion of the insertable camera with the internal driven unit on-board, is generated by spinning the external driving unit and controlling coil input currents. However, in order to accurately actuate the insertable camera to reach its desired orientations, the automatic control of rotation magnetic field generated from the external driving unit is still a major challenge.

In this paper, we develop an automatic rotational control system for a insertable laparoscopic camera capsule with less than 1° control accuracy, as conceptually illustrated in Figure 2. The contributions of this paper beyond our prior work include (1) an abdominal wall thickness estimation system and a current control system were developed for generating appropriate rotational magnetic field to control tilt motion of the camera capsule; (2) an actuation mechanism for the external control unit was designed to enable automatic pan motion control of the capsule; and (3) a fabricated camera system was demonstrated, and experimental analysis was conducted for evaluating the control accuracy of the camera system.

This paper is an extension of our preliminary work.[18] Besides providing through experimental investigations for the camera capsule's rotation control with statistical analysis, this paper presents the tilt motion closed-loop control strategy for the capsule, demonstrates a magnetic field calibration system for the external control unit, and provides the calibrated parameters and experimental evaluations for the modelling accuracy. In addition, the control accuracy of the cEPM actuation mechanism is experimentally tested with statistical results.
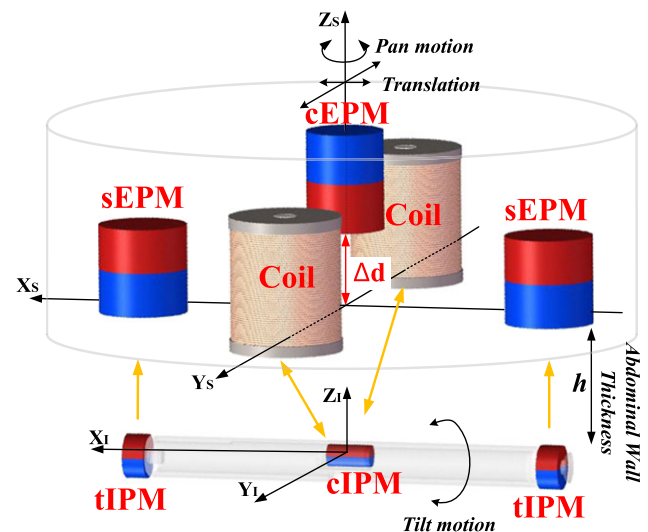

FIGURE 2 Working principle of the camera system. The external control unit generate magnetic forces and torques to control the *in vivo* camera capsule. cEPM: central external permanent magnet; cIPM: central internal permanent magnet; sEPM: side external permanent magnet; tIPM: tail-end internal permanent magnet
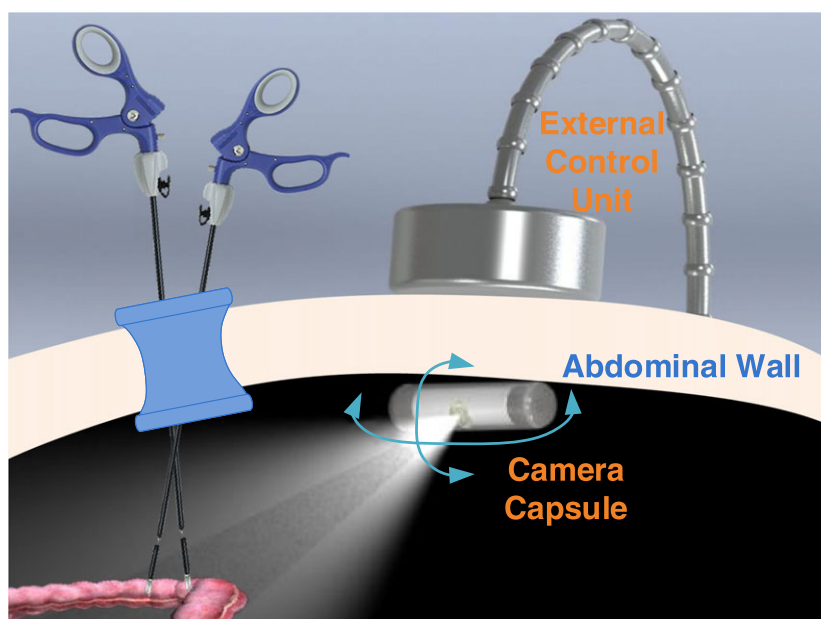

FIGURE 1 Conceptual illustration of the usage of our proposed camera system

The orientation control system hardware architecture is presented in details. The robustness of the abdominal wall thickness sensing system is also validated by statistical methods.

2 | CAMERA CAPSULE ORIENTATION CONTROL CHALLENGES

The research objective of this paper is to enable automatic fine orientation control of the camera capsule system, which consists of tilt motion control and pan motion control. The magnetic actuation mechanism designed in our prior work[17] consists of an external driving unit, namely, a "control unit" and an internal driven unit, namely, a "camera capsule" or simply "capsule," as shown in Figure 1. The control unit positioned externally consists of two coils and three permanent magnets, which are orthogonally arranged. The camera capsule positioned internally consists of three diametrically magnetized permanent magnets. The capsule housing that hosts one magnet in the middle can rotate freely related to the other ring magnets at both ends. The pan motion control requires torque along the capsule Z_l axis, while the tilt motion control requires torque along X_l axis.

A spinning motion of the control unit along Z_l can actuate pan motion of the capsule by coupling the magnetic field of the side external permanent magnets (sEPMs) and the tail-end internal permanent magnets (tIPMs). The directions of the tIPMs are always aligned with the directions of the sEPMs. Therefore, the capsule is fixed on the internal surface of an abdominal wall. The tilt motion can be actuated by the magnetic coupling between the coils and the central internal permanent magnet (cIPM). However, the real situation is that the sEPMs generate strong magnet field at the place where the cIPM locates. Under this condition, the magnetic field from the coils is not strong enough to manipulate the cIPM. The solution is to add a central external permanent magnet (cEPM) with the direction opposite to the sEPMs at the control unit centre. By adjusting the cEPM displacement along Z_s, the magnetic field from the cEPM can balance out the magnetic field from the sEPMs at the location of the cIPM. The cEPM displacement Δd is adjusted according to the control unit-to-capsule distance for minimizing the magnetic field from the EPMs at the location of the cIPM.

3 | CONTROL METHOD OF MAGNETIC ACTUATION MECHANISM

The capsule-to-control unit distance is determined by abdominal wall thickness h. It is required by our system to sense abdominal wall thickness at different locations in real time. Therefore, the *first challenge* to control the camera orientation is how to develop an abdominal wall thickness estimation method and a function $\Delta d = f(h)$. By giving a sensed h, an optimal cEPM displacement $\Delta d = f(h)$ can be calculated with $\Delta d = f(h)$. Based on this step, the *second challenge* of this paper is to develop a closed-loop control scheme for the capsule tilt motion by controlling the coil currents. To generate pan motion of the capsule, the control unit was manually rotated in our previous prototype.[17] In this work, the *third challenge* of this paper is to design an automatic pan motion mechanism in the control unit to control the pan motion of camera capsule.

The orientation control architecture of the camera system is illustrated in Figure 3. The control unit magnetic field is initialized by estimating an abdominal wall thickness h (in Section 3.1), calculating an optimal cEPM displacement Δd according to h (in Section 3.2), and adjusting the cEPM to the displacement Δd (in Section 3.3). The input parameters of the orientation control system are the desired tilt angles θ_d and pan angles φ_d. The control of tilt motion, which is presented in Section 3.4, involves designing the coil current inputs I_{c1} and I_{c2} to minimize the errors between θ_d and real tilt angle θ. For pan motion, the output angle φ is controlled by an actuation mechanism embedded in the control unit, which is presented in Section 3.5.

3.1 | Abdominal wall thickness h estimation

The capsule and the control unit both contact an insufflated abdominal wall internally and externally. The external control unit is anchored and manipulated with a manual goose-neck stand or a robotic arm that provides proper position and orientation of the unit without imposing significant contact force with abdomen. A static capsule with a specific orientation generates static magnetic field. Based on this fact, the capsule magnetic field measured at the control unit side changes by an abdominal wall thickness. The main idea of estimating an abdominal wall thickness is to sense the capsule magnetic field by using a prebuilt
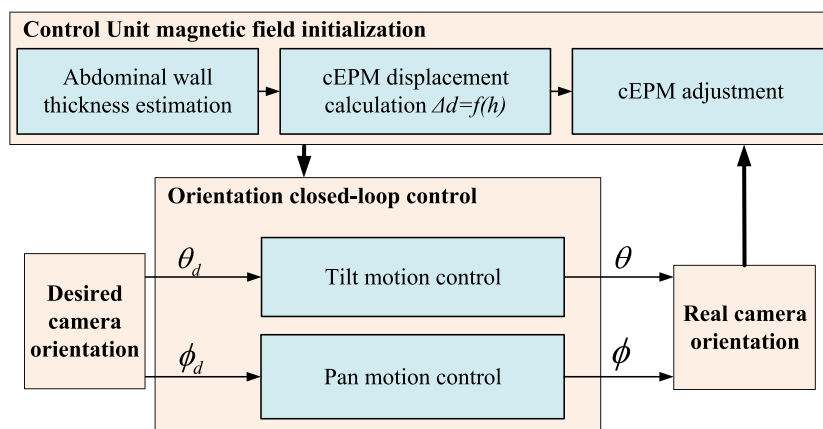

FIGURE 3 The camera system orientation control architecture

capsule magnetic field map, which is with respect to abdominal wall thicknesses or the capsule-to-control unit distances.

There are three challenges to estimate an abdominal wall thickness: (1) Which capsule pose can be most effectively used for building a static magnetic field map? (2) How the magnetic field sensors in the control unit can be configured to detect the magnetic field from the capsule? 3) How the sensed data can be used to estimate the capsule-to-control unit distance? The solutions are presented as follows.

3.1.1 | Static capsule magnetic field generation

The capsule pose determines the static magnetic field distribution. Figure 4 shows two capsule poses for generating symmetric magnetic field maps. The two capsule poses can be actuated by deactivating the control unit coils and adjusting Δd to its maximum and minimum. With the maximum cEPM displacement shown in Figure 4A, the cIPM is dominated by the magnetic field from the sEPMs and aligned with the sEPMs orientation. With the minimum cEPM displacement shown in Figure 4B, the cIPM is dominated by the magnetic field from the cEPM and aligned with the cEPM orientation. The arrows in Figure 4A,B illustrate the magnetic field strength (proportional to the arrow lengths) and magnetic field direction (the arrow directions). It is obvious that the capsule pose in Figure 4A can generate more recognizable magnetic field than that in Figure 4B. Therefore, the control unit initially actuates the cEPM to reach $\Delta d = d_{max}$ for generating the static capsule magnetic field.

3.1.2 | Capsule magnetic field measurement

To measure the magnetic field from the capsule, a set of tri-axis hall effect sensors are installed at the control unit bottom. Because a sensor has its specific measuring range, it is important to select appropriate locations for the sensors to prevent being inundated by the magnetic field from the EPMs. Figure 5A shows the magnetic flux density norm distribution of the EPMs at the control unit bottom. The inundation region in dark red is determined by the measuring ranges of the candidate hall effect sensors. In our design, we apply four tri-axis hall effect sensors, which are symmetrically distributed on the control unit bottom. The black squares S_1, S_2, S_3, S_4 represent the sensor locations, which are outside the inundation region and closest to the capsule.

3.1.3 | h estimation

Figure 5B shows that the tri-axis hall effect sensors detect magnetic field from the capsule at a distance h. Due to the magnetic coupling of the EPMs and the IPMs, the positions between the sensors and the capsule are unchanged in X and Y directions. A magnetic field map f_i represents the relationship between the capsule magnetic field and the capsule-to-control unit distances h_i. The mapping functions f_i represented in lookup tables are developed by recording the magnetic fields with the sensors, while adjusting the capsule-to-control unit distance h.

With the functions f_i and the magnetic fields $\mathbf{B}_i$ sensed by S_i, an abdominal wall thickness can be estimated by

$$h = \frac{1}{N}\sum_{i=1}^{N} f_i(\mathbf{B}_i), \tag{1}$$

where $N = 4$ represents the total number of the hall effect sensors.

3.2 | Optimal cEPM displacement $\Delta d = f(h)$

The cEPM displacement Δd is used to balance out the magnetic field from the sEPMs at the cIPM location. This displacement is effected by an abdominal wall thickness h. Therefore, there is a need to represent Δd as a function of h.

In our prior work,[17] the magnetic field from the coils and the EPMs can be analytically modelled by multi-pair magnetic dipoles as follows

$$\mathbf{B} = \frac{\mu_0}{4\pi} m_{00}\Gamma_{00} + \frac{\mu_0}{4\pi}\sum_{i=1}^{K_m}\sum_{j=1}^{N_m} m_{ij}\Gamma_{ij}, \tag{2}$$

$$\Gamma_{ij} = \frac{\mathbf{Q}_{ij+}}{|\mathbf{Q}_{ij+}|^3} - \frac{\mathbf{Q}_{ij-}}{|\mathbf{Q}_{ij-}|^3}, \tag{3}$$

(A) Static capsule pose when $\mathbf{\Delta d} = \mathbf{d}_{max}$ (B) Static capsule pose when $\mathbf{\Delta d} = \mathbf{0}$
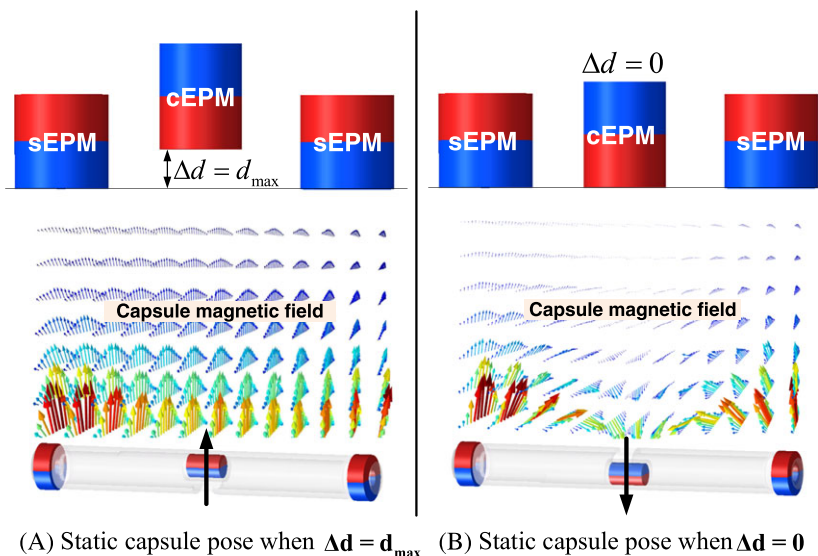
FIGURE 4 Capsule static poses and their magnetic field distributions. A, Capsule pose 1 with the camera opening pointing up; B, capsule pose 2 with the camera opening pointing down. cEPM, central external permanent magnet; sEPM, side external permanent magnet
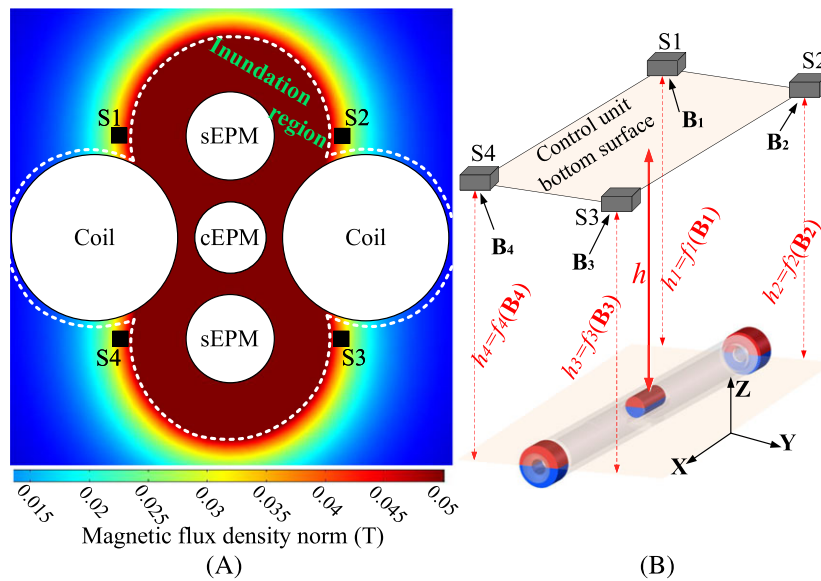
FIGURE 5 Abdominal wall thickness estimation. A, Magnetic flux density norm of the control unit bottom with the selected sensor locations S_1, S_2, S_3, S_4; B, configurations for developing magnetic field maps which is used to estimate an abdominal wall thickness. cEPM, central external permanent magnet; sEPM, side external permanent magnet

where m_{00} and m_{ij} represent the strength of magnetic dipoles; $K_m \times N_m + 1$ represents the total number of magnetic dipoles; $Q_{ij+/-}$ represents a vector from the location of positive/negative magnetic charge to a point in space.

Based on the model in 2, the minimized magnetic field B_{EPM} from the EPMs at the cIPM can be represented by superimposing the magnetic field from each of them.

$$B_{EPM} = R_{s1}B_{s1}(P_{s1}) + R_{s2}B_{s2}(P_{s2}) + R_cB_c(P_c) = 0, \quad (4)$$

where B_{s1}, B_{s2}, and B_c are the magnetic field models of the sEPMs and the cEPM; R_{s1}, R_{s2}, and R_c are the rotation matrices to transform the magnetic field into the same coordinate system; and P_{s1}, P_{s2}, and P_c represent the cIPM coordinates in the local frames of the EPMs;

Because h and Δd are both in 4, it is desired to explicitly formulate a function as $\Delta d = f(h)$. However, due to the non-linear property of 2 and 4, it is difficult to have such a function. An alternative way to develop this function is to build a lookup table by giving a range of abdominal wall thickness values h. After searching for Δd that satisfies 4, the optimized Δd values are stored in the lookup table. To this end, the optimal vertical displacement of cEPM Δd can be identified in real time for different h values.

3.3 | cEPM actuation mechanism

According to the estimated h from 1, the cEPM displacements $\Delta d = f(h)$ are determined in Section 3.2. To actuate the cEPM to the displacement Δd, we need to design an adjusting mechanism in the control unit. Considering the strong magnetic coupling between the cEPM and the sEPMs, the mechanism should be able to provide sufficient lifting force for the cEPM and keep the whole control unit as compact as possible.

Figure 6 illustrates the design of the cEPM actuation mechanism in the control unit. The design has two major considerations: (1) the actuation force for the cEPM movement can be efficiently provided by
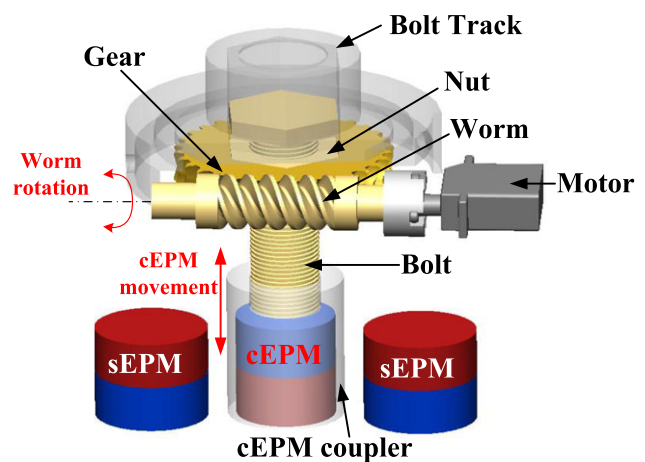

FIGURE 6 cEPM displacement actuation mechanism in the control unit. cEPM, central external permanent magnet; sEPM, side external permanent magnet

the worm and gear mechanism and (2) the self-locking function of the design enables the cEPM to keep still when the motor is unactuated. The bolt that connects with the cEPM by using a coupler is actuated by the gear rotation. The bolt track restricts the bolt rotation and keeps the bolt and the cEPM moving vertically.

3.4 | Tilt motion control

3.4.1 | Capsule protection shell

The camera design in our prior work[17] may potentially get blurred by peritoneal fluid due to the direct contact with an abdominal wall. To address this issue, a transparent shell is applied to prevent the camera lens from contacting with tissue and also to maintain imaging quality, as illustrated in Figure 7A-5. Two ceramic bearings (Figure 7A-7) and two tIPM shafts (Figure 7A-6), which are fixed in the shell caps (Figure 7A-1), are used for hanging the camera housing (Figure 7A-3)
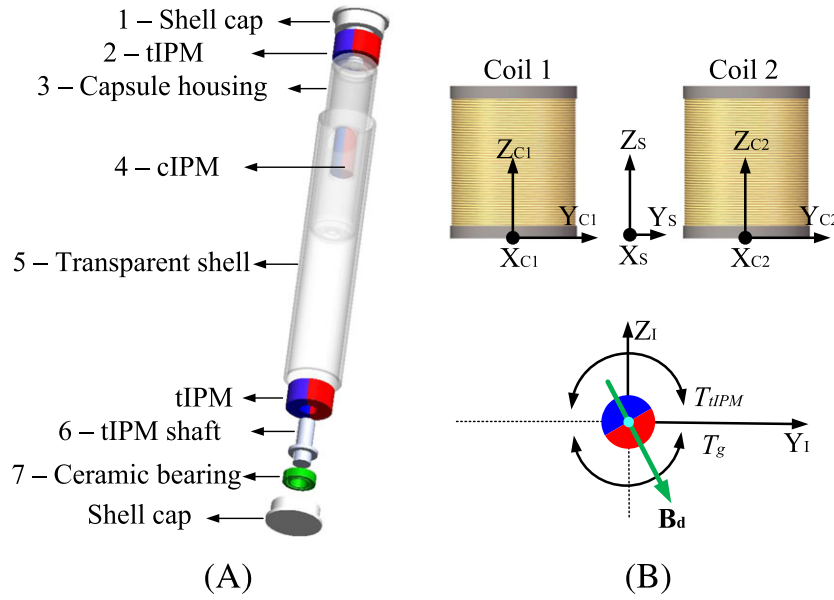
FIGURE 7 A, Conceptual illustration of the capsule design. B, Capsule tilt motion control with the coils. cIPM, central internal permanent magnet; tIPM, tail-end internal permanent magnet

inside the transparent shell with no contact. This design provides the camera smooth rotation inside the shell when rotational torque is exerted on the cIPM (Figure 7A-4). Another benefit of this design is to make the laparoscopic camera reusable by depositing the shell after use and subsequently reduces surgery cost.

The new capsule design insulates the camera lens from contacting with an abdominal wall. It makes the capsule housing free of frictional torque from an abdominal wall during tilt motion. Compared with the tilt motion control method developed in Liu et al,[17] this new capsule design can significantly reduce the motion control complexity and improve the control robustness, which has been experimentally proved in Section 4.9. The detailed information to control the tilt motion of the new capsule are as follows.

3.4.2 | Control with electromagnetic coils

The camera tilt motion is activated by the magnetic coupling between the coils and the cIPM. I_{c1} and I_{c2} represent current inputs of the coils, and θ represents a tilt angle.

The factors that impact on the camera tilt motion need to be firstly considered. After estimating an abdominal wall thickness h and actuating the cEPM displacement Δd, the EPMs have ignorable impact on the tilt motion of the cIPM. Beside the control inputs I_{c1} and I_{c2}, the tilt motion of the cIPM is also affected by T_g and T_{tIPM}, which are the torques due to the robot gravity along X_I and the magnetic torque on the cIPM from the tIPMs along X_I respectively. As illustrated in Figure 7B, T_g and T_{tIPM} are always in opposite directions and are cancelled by each other according to our preliminary experimental investigation. Therefore, the camera tilt angle aligns with the direction of the magnetic field generated by the coils. The objective to control the camera tilt motion is to determine I_{c1} and I_{c2} for generating a magnetic field with the direction θ at $\mathbf{P}_s$ in $\Sigma_S\{X_S, Y_S, Z_S\}$, where $\mathbf{P}_s$ is the location of the cIPM.

The relationship between the current inputs and desired magnetic field directions can be formulated by 5 in Σ_S as follows

$$\underbrace{(\mathbf{R}_{C1}\mathbf{B}_c^u)}_{\mathbf{B}_{c1}^S}I_{c1} + \underbrace{(\mathbf{R}_{C2}\mathbf{B}_c^u)}_{\mathbf{B}_{c2}^S}I_{c2} = \underbrace{\mathbf{R}_I^S \mathbf{R}_{Ix}(\theta)\mathbf{B}^{-z}}_{\mathbf{B}_d}, \quad (5)$$

where $\mathbf{R}_I^S \in \mathbb{R}^{3\times3}$ represents a rotation matrix from $\Sigma_I\{X_I, Y_I, Z_I\}$ to Σ_S. According to the setting of Σ_S and Σ_I in Figure 7B, $\mathbf{R}_I^S$ is an identity matrix. $\mathbf{R}_{Ix}(\theta) \in \mathbb{R}^{3\times3}$ represents the rotation matrix along X_I with θ as a variable. $\mathbf{B}^{-z} \in \mathbb{R}^{3\times1}$ denotes a unit vector pointing in $-Z_I$. $\mathbf{B}_{c1}^S, \mathbf{B}_{c2}^S \in \mathbb{R}^{3\times1}$ denote the unit-current magnetic field of the coils at $\mathbf{P}_s$ in Σ_S. $\mathbf{B}_d \in \mathbb{R}^{3\times1}$ denotes the desired magnetic field direction as shown in Figure 7B. Benefiting from the magnetic field model in 2, $\mathbf{B}_{c1}^S, \mathbf{B}_{c2}^S$ can be computed in real time.

Considering the x components in $\mathbf{B}_{c1}^S$, $\mathbf{B}_{c2}^S$, and $\mathbf{B}_d$ are zeros, 5 is reformulated as

$$\mathbf{B}_d^{yz} = \mathbf{B}_c^{S_{yz}}\mathbf{I}_c, \quad (6)$$

where $\mathbf{B}_c^{S_{yz}} = [\mathbf{B}_{c1}^{S_{yz}}, \mathbf{B}_{c2}^{S_{yz}}] \in \mathbb{R}^{2\times2}$, $\mathbf{B}_d^{yz} \in \mathbb{R}^{2\times1}$, $\mathbf{I}_c = [I_{c1}, I_{c2}]^T \in \mathbb{R}^{2\times1}$. Because $\mathbf{B}_c^{S_{yz}}$ has a full row rank, the current input vector $\mathbf{I}_c$ can be found in 7 by applying pseudoinverse to 6

$$\mathbf{I}_c = (\mathbf{B}_c^{S_{yz}})^T(\mathbf{B}_c^{S_{yz}}(\mathbf{B}_c^{S_{yz}})^T)^{-1}\mathbf{B}_d^{yz}. \quad (7)$$

To achieve high accuracy tilt motion control, a closed-loop control scheme is developed as illustrated in Figure 8. Given a desired tilt angle θ_d, a current vector is calculated by $\mathbf{I}_c = \tilde{f}(\mathbf{P}_s, \tilde{\theta})$, which is another representation of 7. Because the solution of 7 only provides the ratio of I_{c1} and I_{c2}, the input current vector is amplified with I_{max} to maximize the generated magnetic field. A current input trajectory $\mathbf{I}_c^{max}(t)$ can thus be developed by a given time period ΔT, and applied to the capsule. The arrived tilt angle θ at the end of $\mathbf{I}_c^{max}(t)$ is measured by a tilt angle sensor for feedback. If $\Delta\theta = |\theta_d - \theta|$ is smaller than a given threshold δ_θ, the tilt angle control process is complete. Otherwise, an adjusted tilt angle $\tilde{\theta} = \theta_d \pm \Delta\theta$, where $\Delta\theta$ is a small step angle, is served as a new input to calculate $\mathbf{I}_c$.
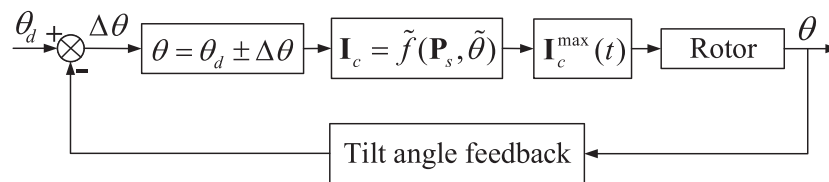
$$\theta_d \xrightarrow{+} \xrightarrow{\Delta\theta} \boxed{\theta = \theta_d \pm \Delta\theta} \rightarrow \boxed{\mathbf{I}_c = \tilde{f}(\mathbf{P}_s, \tilde{\theta})} \rightarrow \boxed{\mathbf{I}_c^{\max}(t)} \rightarrow \boxed{\text{Rotor}} \xrightarrow{\theta}$$

$$\boxed{\text{Tilt angle feedback}}$$

FIGURE 8 Block diagram of the camera tilt motion control
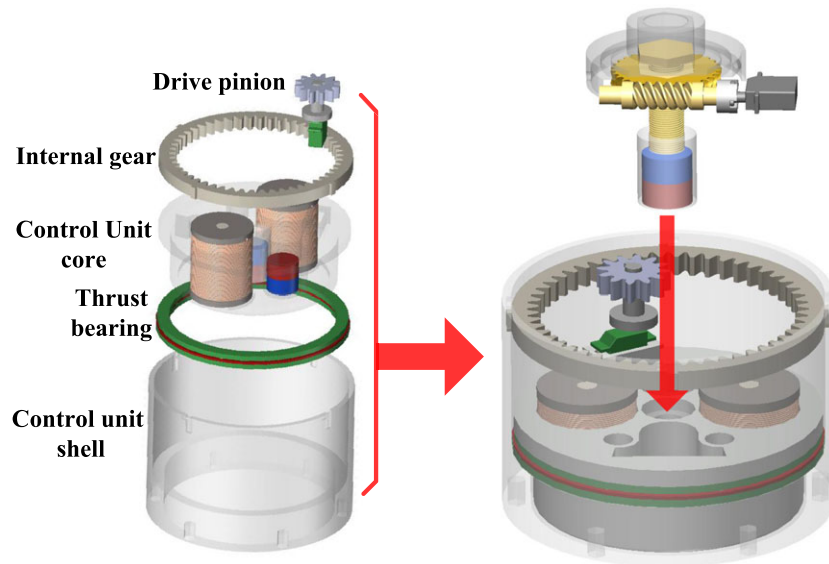
FIGURE 9 Pan motion actuation mechanism in the control unit

3.5 | Pan motion mechanism

To control the pan motion automatically, it is desired to design an actuation mechanism that can generate rotational motion of the control unit. Figure 9 demonstrates the pan motion mechanism in the control unit. The mechanism controls rotational motion of the control unit core, which is sitting inside the control unit shell. A motor driven spur gear is fixed on the control unit core, while an internal gear is attached on the internal surface of the control unit shell. The control unit core can thus be actuated by the relative motion of the spur gear and the internal gear. To keep smooth relative rotation between the control unit core and the control unit shell, a thrust bearing is applied at their contact surfaces. The cEPM actuation mechanism presented in 3.3 is fixed on the top of the control unit core, and the cEPM is inserted in the middle hole on the control unit core.

4 | PROTOTYPE DEVELOPMENT AND EXPERIMENTAL INVESTIGATION

4.1 | Experimental platform

Figure 10A shows the overview of the experimental environment. The major parts of the camera system were fabricated by a 3D prototyping machine (Fortus 400mc, Stratasys Inc). To simulate the viscoelastic properties of a real insufflated abdominal wall (average Young modulus 32.5 kPa),[14] a viscoelastic material Durometer 40 (Young modulus of 27.57 kPa at 15% deflection, Sorbothane, Inc.) was applied. The initial abdominal wall thickness was 26 mm (tissue layer, 15 mm;

support layer, 11 mm). To increase the abdominal wall thickness for experimental studies, a vertical control unit positioning mechanism in Figure 10A was applied. A silicone oil–lubricated capsule-tissue contact layer was added to the bottom of the viscoelastic material for mimicking an internal abdominal wall surface.

4.1.1 | Control system hardware architecture

Figure 11 shows the hardware architecture for the camera orientation control system. A tethered current control system was developed based on pulse width modulation (PWM). The system consists of a micro-controller (STM32F4Discovery, STMicroelectronics Inc.) to generate PWM signals, two PWM amplifiers (L6205 DMOS Full Bridge Driver, STMicroelectronics Inc.) to amplify the signals, a power supply for powering up the amplifiers, and a PC to send control command to the micro-controller via serial communication. The abdominal wall thickness sensing system was implemented by setting four sets of tri-axis hall effect sensors to detect magnetic field from the capsule. The detected analog magnetic field signals were converted into digital signals through four sets of AD converters. In order to provide closed-loop feedback sensing, at this stage, we applied an external camera and on-board sensor to acquire real time orientation feedback.

4.2 | Control unit fabrication

4.2.1 | cEPM adjusting mechanism

The fabrication of the cEPM adjusting mechanism that is proposed in Section 3.3 involves two concerns: (1) The mechanism has to provide
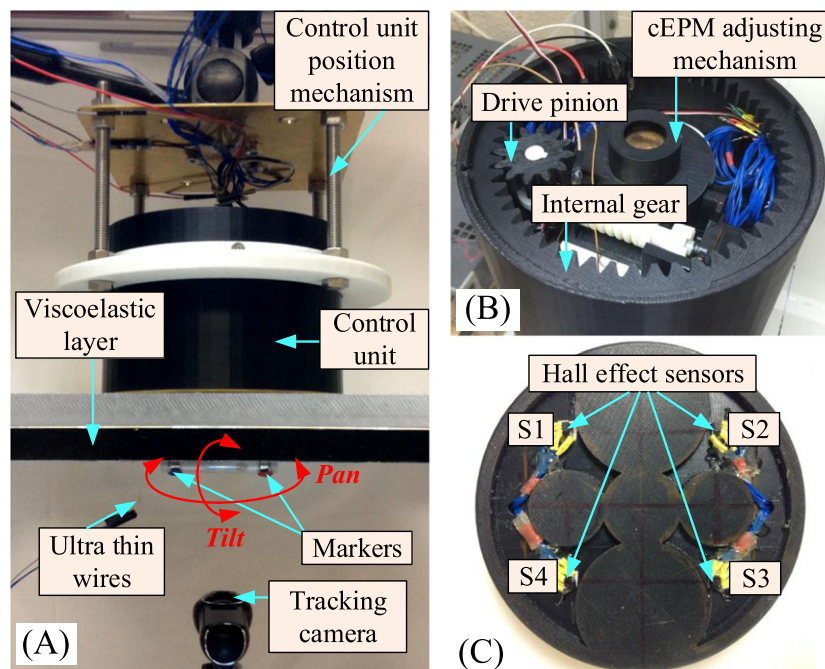
FIGURE 10 Experiment platform set-up and the control unit configuration. A, Overview of the camera orientation control system. B, Demonstration of the pan motion mechanism and the central external permanent magnet (cEPM) actuation mechanism. C, Magnetic field sensing system
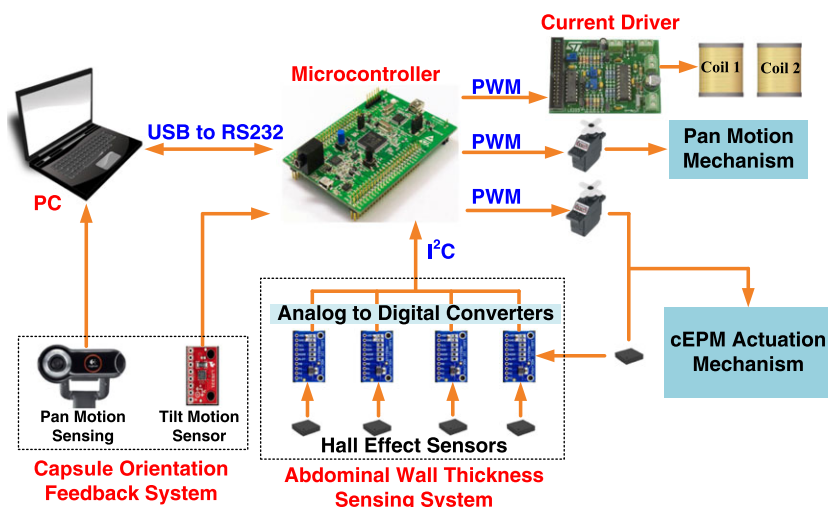

FIGURE 11 Control system hardware architecture. cEPM, central external permanent magnet; PWM, pulse width modulation

sufficient lifting force to overcome the magnetic force between the cEPM and the sEPMs; and (2) the cEPM has to be accurately controlled to the desired displacement Δd.

The design objective is to make the cEPM adjusting mechanism compact enough to fit in the control unit shell (external diameter, 164 mm; height, 109 mm). The worm in Figure 12A is with pitch diameter of 12.19 mm, outside diameter of 15 mm, number of threads of $N = 3$, and worm length of 25 mm. The gear is with 32 teeth, pitch diameter of 45 mm, outer diameter of 49.25 mm, and face width of 10 mm. The nut that fixed at the gear centre is used for generating vertical displacements of the bolt by rotating the gear and the nut. The hex nut is with height of 13.89 mm and diameter of 15.875 mm. The bolt is matching with the nut with thread length of 53 mm and screw pitch of $p = 2$ mm. According to our preliminary experiments,

the maximum force needed to pull out the cEPM from the magnetic coupling between the cEPM and the sEPMs is about $F = 50$ N. The required motor torque M_T can be estimated by

$$M_T = \frac{F \cdot p}{2\pi \cdot \eta_s \cdot \eta_{wg} \cdot r}, \tag{8}$$

where η_s and η_{wg} are the efficiencies of the screw and the worm-gear respectively; $r = 32/3$ is the ratio of the worm gear. M_T is estimated as 0.149 Nm by conservatively assuming $\eta_s = 10\%$ and $\eta_{wg} = 10\%$. A servo motor (S3156, Futaba Inc) in Figure 12A, which can provide 0.196 Nm at 4.8 V, was modified into continuous rotation for our application. To avoid influencing the magnetic field of the control unit, the silicone brass screw and nut (Bolt Depot, Inc) were selected for the design.
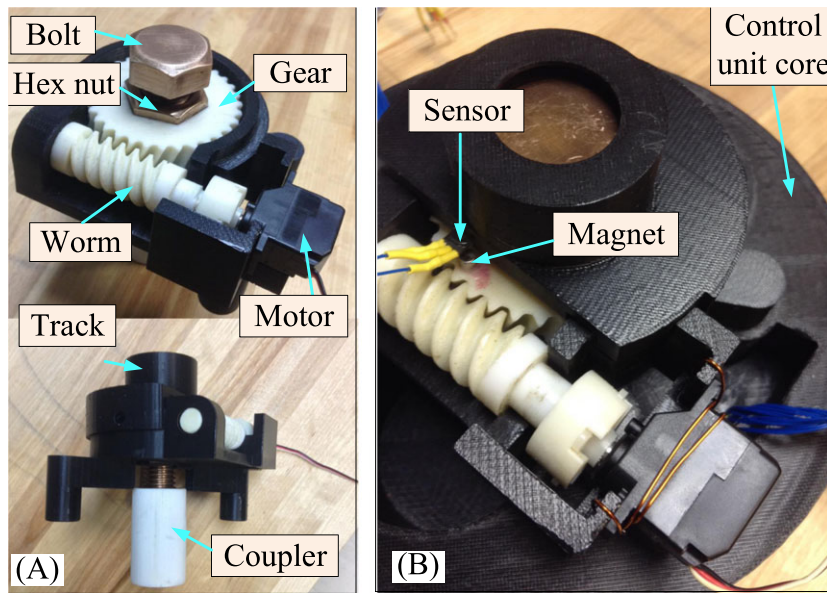
FIGURE 12 Configurations of the central external permanent magnet adjusting mechanism
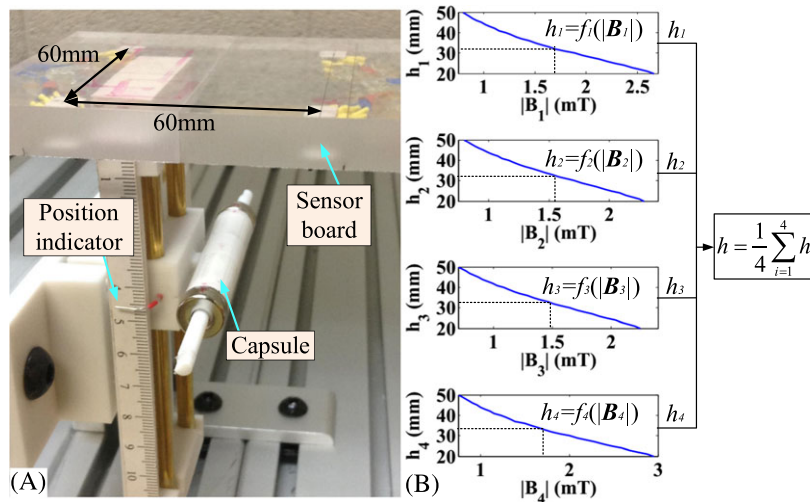

FIGURE 13 Experimental configuration for developing abdominal wall thickness estimation functions

Figure 12B shows the assembly of the cEPM adjusting mechanism with the displacement sensing system on the control unit core that houses the EPMs and the coils. To sense the cEPM vertical displacements, a magnetic encoder is designed by using four tiny cylindrical permanent magnets symmetrically distributed on the gear surface. A single hall effect sensor (CYL8405, Chenyang-Technologies GmbH& Co. KG) is applied to pick up the magnetic field signal from the magnets to measure the gear rotation. The screw travels 2 mm when the gear generates a full rotation. Four magnets can thus provide 0.5 mm control resolution.

4.2.2 | Abdominal wall thickness sensing system

According to the design in Section 3.1, the magnetic field sensing system was implemented at the bottom of the control unit core, as illustrated in Figure 10C. The bottom of the control unit core is carved around the EPMs and the coils with 5-mm depth for installing magnetic

field sensors. Four sets of tri-axis hall effect sensors with measuring ranges 0 to 64 mT and sensitivities about 50 mV/mT were symmetrically fixed in the carved bottom. To enable the system to measure tiny changes of the capsule magnetic field, the measured signals were converted to digital signals with sensing resolution 0.01 mT by using a 16-bit ADC (ADS1115, Texas Instruments Inc.).

The estimation function in 1 was implemented by the data acquired from the experimental set-up in Figure 13A, which has the same sensor configuration as that in the control unit in Figure 10C. The capsule with the pose demonstrated in Figure 4B was fixed on a vertical positioning stage for adjusting the distance between the capsule and the sensors. Figure 13B shows the estimation functions $f_i, (i = 1, 2, 3, 4)$, which record the norms of the magnetic flux densities $|\mathbf{B}_i|$ and the vertical distances h_i between the capsule and the sensors S_i. An average value of h_i was used as the final estimated abdominal wall thickness h to improve the robustness of this method.

4.3 | Control unit dimensions

The fabricated control unit is demonstrated in Figure 10B. The internal gear has 52 teeth with pitch diameter of 132 mm, major diameter of 139.4 mm, and minor diameter of 128 mm. The drive pinion has 12 teeth with pitch diameter of 30.48 mm, major diameter of 36.56 mm, and minor diameter of 25.13 mm. The face widths of the internal gear and the drive pinion are both 10 mm. The control unit shell is with external diameter of 164 mm and height of 109 mm. The thrust bearing with inner diameter of 133.6 mm and outer diameter of 154.6 mm sits inside the control unit shell with 30-mm distance to the shell bottom. A modified digital servo motor, which is identical to the motor applied on the cEPM adjusting mechanism, is fixed in the control unit core and connected with the drive pinion. A brass board with diameter of 164 mm and thickness of 1.64 mm was applied at the bottom of the control unit shell for protecting the control unit core and avoiding magnetic field influence between the capsule and the control unit.

4.4 | Magnets and coil selection

The magnets applied in the control unit are all axially magnetized cylindrical shape with two different dimensions. The sEPMs are 25.4 mm in diameter, 25.4 mm in length, and 1.43 T of magnetic remanence. The cEPM is 22.22 mm in diameter, 28.57 mm in length, and 1.43 T of magnetic remanence. The magnets in the capsule are all diametrically magnetized. The tIPMs are ring-shaped with 12.7 mm in outer diameter (OD), 4.75 mm in inner diameter (ID), 6.35 mm in thickness, and 1.32 T of magnetic remanence. The cIPM is cylindrical shape with 6.35 mm in diameter, 12.7 mm in length, and 1.32 T of magnetic remanence (K&J Magnetics, Inc). Two iron-core coils are applied in our design with OD of 50 mm, ID of 10 mm, height of 50 mm, and 2000 winding turns.

4.5 | Capsule dimensions

Figure 14 shows the fabricated dummy camera with the disassembled parts. The outer diameter of the transparent shell (MOCAP, Inc.) determines the camera diameter as 14.52 mm, which can fit in a standard trocar with diameter of 12 to 15 mm. The miniature ceramic ball bearings (NationSkander California Corp.) enable smooth rotation of the camera housing inside the transparent shell. The bearings are 5 mm in inner diameter, 9 mm in outer diameter, and 3 mm in thickness.

4.6 | Calibration of magnetic field models

The control unit magnetic field model developed in Section 3.2 was formulated by 2 with parameters m_{00}, m_{i1}, $(i = 1, \ldots, 10)$. Due to the imperfection of the coil wrapping, the iron cores, and the permanent magnets, the model calibration was performed by using experimental data. Figure 15A shows the experiment set-up for magnetic field calibration, which consists of a transparent board to support the EPMs or the coils, one X-Z position stage, and hall effect sensors for three axes magnetic field sensing. Figure 15B,C show the magnetic flux density norm comparison results of the experimental data and the magnetic field models.

Figure 15B illustrates the calibrated coil magnetic field model (the blue line) with unit-current input based on the experiment data (the blue circles). The red line and the red circles illustrate the magnetic field comparison result between the predicted magnetic field with calibrated parameters in Table 1 and the sensed experiment data when $I = 0.5$ A. This result validates the linear relationship between the coil input current and the generated magnetic field strength. Figure 15C shows the magnetic field comparison result between the EPMs magnetic field model prediction data and experiment data with the cEPM vertical displacements $\Delta d = 1, 3, 5,$ and 7mm. The coincidences of the model prediction data and the experiment data at $B_{norm} = 0$ with various Δd validate the optimal displacement function $\Delta d = f(h)$ developed in Section 3.2. The average errors of the magnetic field models demonstrated in Figure 15B,C were 0.11% and 0.23%, respectively. The calibrated parameters of the EPMs and the coils are shown in Table 1.
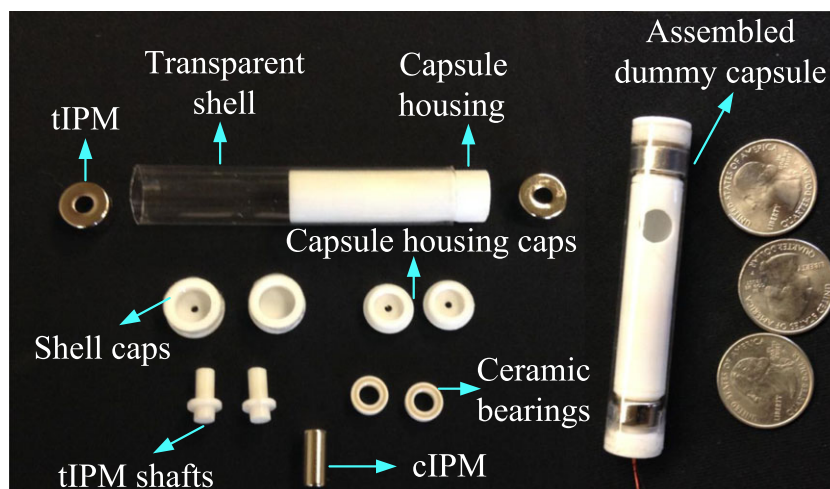

FIGURE 14 The disassembled dummy capsule parts and the assembled dummy capsule. cIPM, central internal permanent magnet; tIPM, tail-end internal permanent magnet
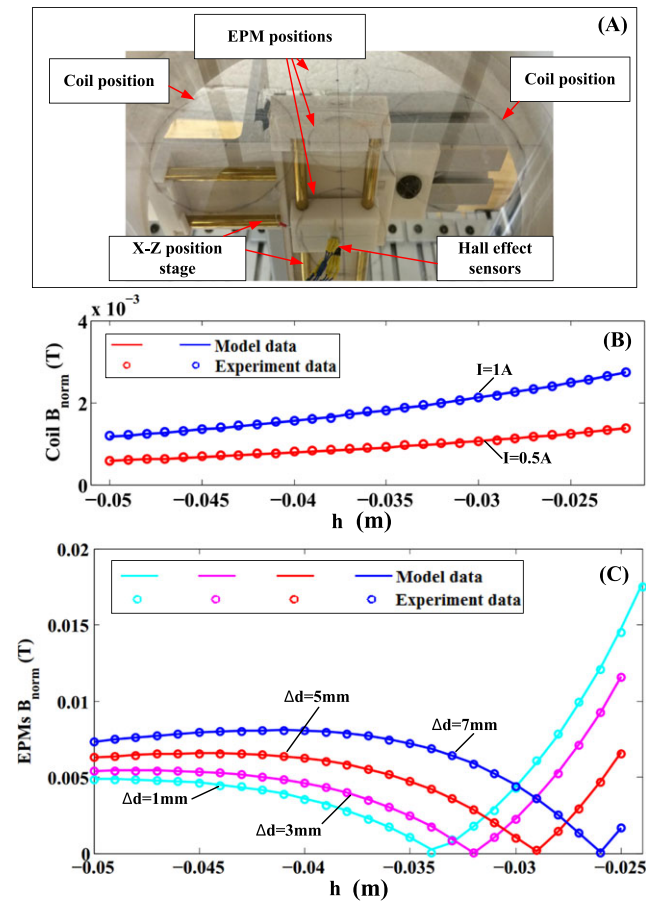
FIGURE 15 Experimental set-up for calibrating the magnetic field models of the control unit. A, Magnetic field calibration platform with a supporting board for magnets/coils, X-Z position stage, and magnetic field sensors. B, Experimental results for the coils calibration. C, Experimental results for the EPMs calibration. EPM, external permanent magnet

4.7 | Control of cEPM displacements

Figure 16 shows the investigation of the control accuracy for the cEPM adjusting mechanism developed in Section 4.2.1. The measured displacement from a calliper served as the benchmark. The desired cEPM displacements were set from 2 to 10 mm with 2-mm intervals. For each test, the cEPM displacement was initially set at $\Delta d = 0$. The results show that the maximum errors of all group tests were within 0.4 mm, which provides sufficient control accuracy for the camera system. As the cEPM displacements travelled from 2 to 10 mm, the errors were accumulated. The accumulated error can be limited within 0.37 mm by resetting the displacement counter when the minimum or the maximum displacement is reached.
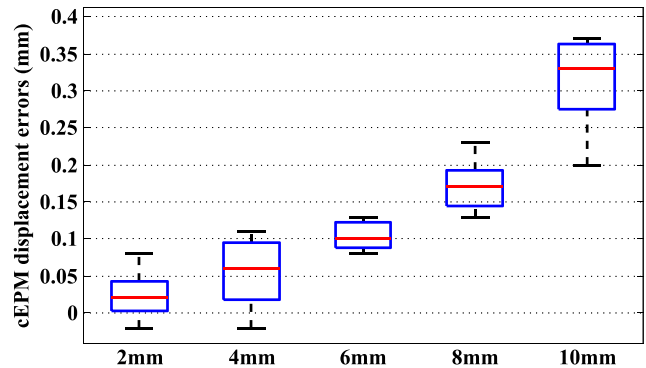

FIGURE 16 Investigation of the central external permanent magnet (cEPM) displacement control accuracy. Desired cEPM displacements Δd were set from 2 to 10 mm

4.8 | Evaluation of abdominal wall thickness estimation method

Figure 17 shows the experiment set-up and experiment results for evaluating the abdominal wall thickness estimation method developed in Section 3.1. To investigate the accuracy and robustness of the proposed method, the experiment was divided into two groups, which are (1) the estimation under the impact of the EPMs and (2) the estimation without the impact from the EPMs. The two-group experimental set-ups can be achieved by putting or removing the EPMs in the control unit core with the coils deactivated, as shown in Figure 17A. In both experiment groups, the capsule with the pose demonstrated in Figure 4A was attached to a Z-axis positioning stage under the control unit core. To test the estimation robustness, the control unit core was rotated within the range of ±20° during each estimation process. Figure 17B shows the capsule-to-control -unit distance estimation errors at 25, 30, 35, 40, 45, and 50 mm. The mean absolute errors (MAEs) and the standard deviations (SDs) of the two-group experiments under different testing distances are shown in Table 2. The data show that the abdominal wall thickness estimation system can provide sub-millimetre accuracy. To investigate the differences of the estimation errors between the two-group experiments, two-sample t tests were applied to compare the MAEs and the SDs. The P values for the MAEs and the SDs were 0.6693 and 0.4210, respectively, which indicate that the differences were considered to be statistically insignificant.

4.9 | Camera orientation control

The closed-loop control of the camera motion requires sensing systems for tilt angles and pan angles. Due to the lack of on-board wireless inertial measurement sensors at the current stage, separate tethered motion feedback systems were designed for pan and tilt motion, as
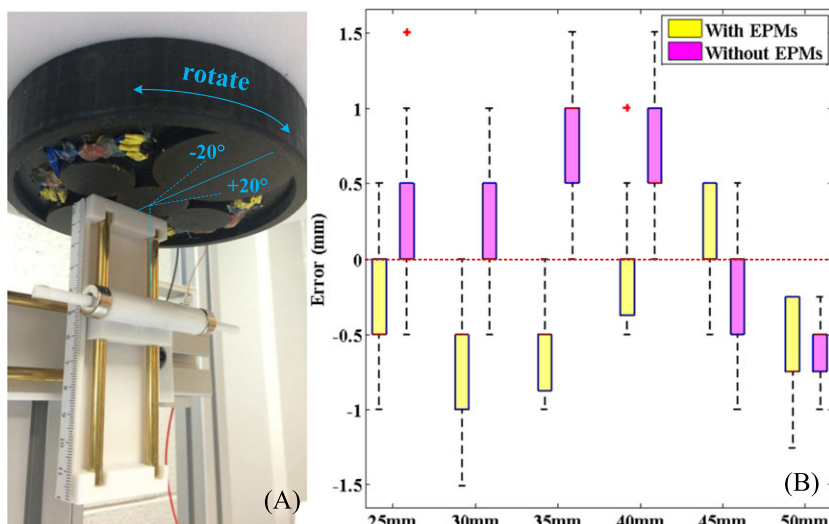
TABLE 1 Calibrated parameters of the sEPMs, the cEPM, and the coils

	m_{00}	m_{11}	m_{21}	m_{31}	m_{41}	m_{51}	m_{61}	m_{71}	m_{81}	m_{91}	$m_{10,1}$
sEPM	2.479	2.676	2.516	2.294	2.063	1.894	1.759	1.536	1.225	1.136	1.252
cEPM	2.493	2.456	2.436	2.393	2.349	2.305	2.264	2.233	2.209	2.193	2.185
Coil	2.494	2.401	2.394	2.398	2.394	2.403	2.395	2.398	2.398	2.393	2.401

Abbreviations: cEPM, central external permanent magnet; sEPM, side external permanent magnet. Units: [$A \cdot m2$].

FIGURE 17 Abdominal wall thickness estimation method investigation. A, Experimental set-up. B, Two-group experimental results for the estimations with/without the magnetic field influence from the external permanent magnets (EPMs)

TABLE 2 MAE and SD of the estimated capsule-to-control unit distances

Dist, mm	With EPMs		Without EPMs	
	MAE, mm	SD, mm	MAE, mm	SD, mm
25	0.2672	0.3531	0.2368	0.5506
30	0.6118	0.3025	0.1771	0.2989
35	0.5256	0.3431	0.7216	0.3678
40	0.0116	0.3856	0.6910	0.3807
45	0.2	0.2857	0.1684	0.3832
50	0.5682	0.2424	0.5729	0.1943

Abbreviations: EPM, external permanent magnet; MAE, mean absolute error; SD, standard deviation.
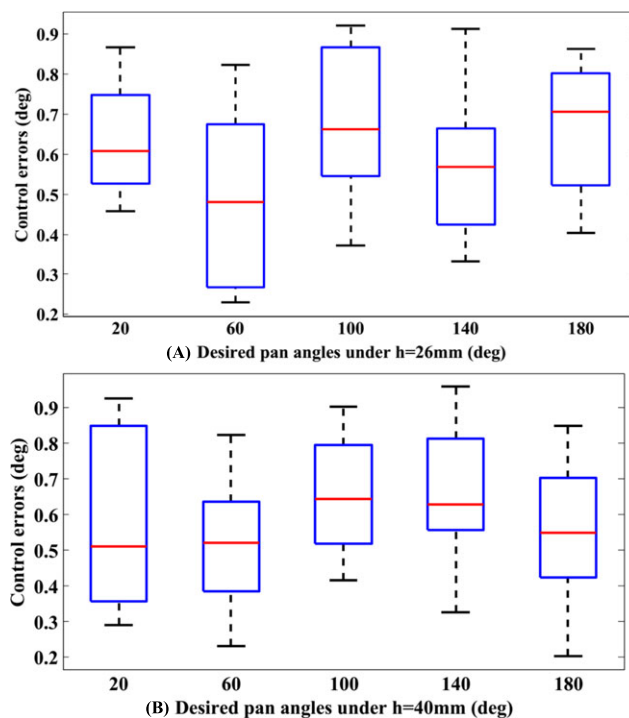

FIGURE 18 Pan motion closed-loop control by setting desired angles from 20° to 180°. A, Under 26-mm abdominal wall thickness; B, under 40-mm abdominal wall thickness

shown in Figure 11. The tilt motion sensing system applied a tri-axis accelerometer (LIS331HH, STMicroelectronics Inc.), which is fixed inside the camera housing. To minimize the impact on the camera tilt motion from the wires, 42 AWG enamelled copper wires with diameter of 0.066 mm (Remington Industries, Inc.) were applied for power supply and data transmission. The pan motion sensing system applied a webcam (Logitech Pro 9000) under the capsule to track the positions of two colour markers on the transparent shell of the dummy camera. The current inputs of the two coils are limited at $|I_{max}| = 1.5\,A$ to prevent coil overheating.

The camera orientation control resolution depends on the error thresholds for tilt motion (δ_θ) and pan motion (δ_φ). An excessively fine orientation control resolution, such as 0.1°, is not only unnecessary for a laparoscopic surgery but also challenges the system's real-time performance. In this work, δ_θ and δ_φ are both set as 1° to achieve a balance between high control resolution and burden on system's real-time performance.

Figure 18 and Figure 19 demonstrate the control accuracies of the orientation control system under two different abdominal wall thicknesses, which are 26 and 40 mm. To test the pan motion control accuracy, desired angles are set at 20°, 60°, 100°, and 120° with initial angles set at 0°. Ten trials were executed for each desired control angle. The statistic results in Figure 18 show that the camera pan motion can be successfully controlled with an average control error 0.594°. To test the tilt motion control accuracy, desired angles are sampled from 10° to 70° with an interval as 10°.

Figure 19 shows that all the control errors of tilt motion are all limited within 1° with an average error as 0.524°. Figure 20 shows that the tilt motion control trajectories for the desired tilt angles at 15°, 45°, and 75° took 0.93, 1.74, and 1.99 seconds, respectively, to reach steady states.
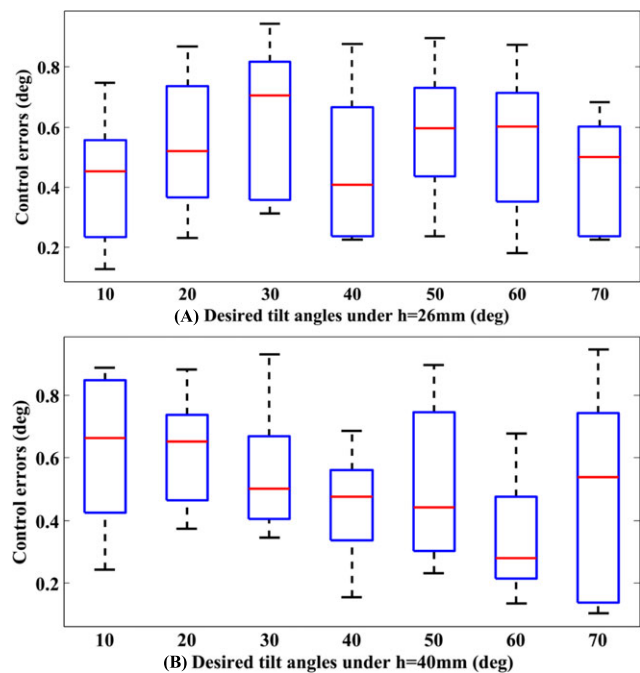
FIGURE 19 Tilt motion closed-loop control by setting desired angles from 20° to 180°. A, Under 20-mm abdominal wall thickness; B, under 40-mm abdominal wall thickness
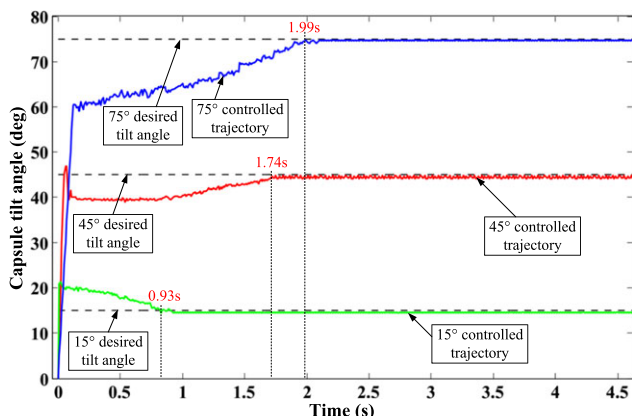

FIGURE 20 Tilt motion control trajectories under an abdominal wall thickness as 40 mm

5 | DISCUSSION

As shown in Figure 15C, the optimal displacement of the cEPM is $\Delta d = 1$ mm when the abdominal wall thickness is about 34 mm.

Because the minimum value of Δd is zero, the cEPM cannot be further adjusted when the abdominal wall thickness is over 35 mm. However, this does not result in a problem to control the camera tilt motion. The cEPM displacement $\Delta d = 0$ and the increased abdominal thickness work together to reduce the magnetic field on the cIPM from the EPMs. The effectiveness of the tilt motion control with a 40-mm abdominal wall thickness has been validated in Figure 19B. Combined tilt and pan actuation of capsule was experimented for 0° to 75° tilt motion and 0° to 180° pan motion, and results are shown in Figure 21.

To enable sufficient range of motion for inspecting an abdominal cavity, a minimum range of the camera tilt motion is required. This range of motion depends on the field of view of an on-board camera module that will be integrated in our future work. For example, by conservatively assuming the camera field of view as 50°, the minimum required tilt angle is 65°, which can be easily achieved by our design as illustrated in Figure 19.

Considering some patients, who are obese or skinny, with their abdominal thicknesses out of the normal range 20 to 40 mm, the prototype design in this paper may not function appropriately. In that case, the control unit parameters can be designed according to the largest abdominal wall thickness, such as 70 mm. To make the robot system function normally when an abdominal thickness is smaller than 70 mm, a lifting mechanism in the control unit can be developed to increase the capsule-to-control unit distance to the normal working range.

It is noteworthy to further consider the magnetic field effect on other surgical tools during laparoscopy surgery. Even though the generated magnetic field provides enough force for fixation and manipulation of the camera capsule in the range of 20 to 50 mm, the magnetic field drastically decreases in further distances from external control unit, due to its nature. As shown in Figure 2, independent manipulation of camera capsule with respect to other instruments reduces the possibility of interference with other instruments.

In order to insert/remove the camera capsule into/from the abdominal cavity though a single incision, a small continuum manipulator, which is capable of manipulating objects though an incision, will be designed with a gripper and a camera installed at the tip. Due to the strong magnetic fields surrounded by the capsule and the control
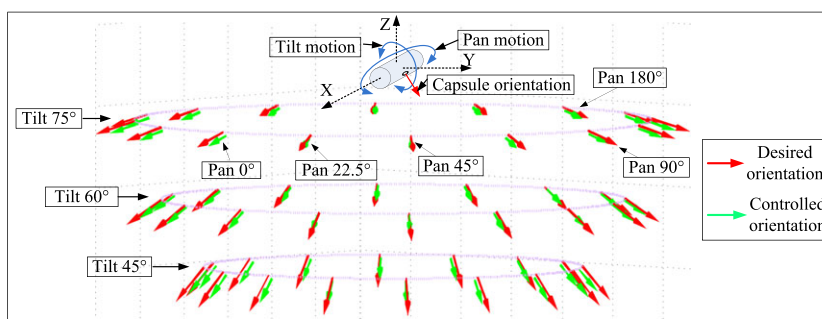

FIGURE 21 Tilt and pan motion experiment results under an abdominal wall thickness as 40 mm

unit, the material of the continuum manipulator should be selected as non-ferrous metals or plastic materials to avoid the magnetic field influence. To guarantee that the continuum manipulator can provide sufficient force for placing and retrieving the robot, a minimum of 30 g force should be considered to design the manipulator. In case of sudden removal of control unit and capsule fall inside abdominal cavity consequently, the continuum manipulator's gripper can be used for picking up the capsule. The manipulating feature of this system eases the removal by controlling the orientation of camera capsule through the trocar/incision.

6 | CONCLUSION AND FUTURE WORK

In this paper, a closed-loop control system of a novel insertable laparoscopic camera has been presented to enable 2D orientation control, which consists of tilt motion control and pan motion control. The magnetic actuation mechanism features a unified control of anchoring, navigating, and rotating the camera without on-board electric motors. The tilt motion control was achieved by developing a control unit magnetic field function, an abdominal wall sensing system, and a cEPM adjusting mechanism with 0.5-mm resolution to generate optimal magnetic field from the EPMs. A closed-loop control scheme was presented to control current inputs of the coils in the control unit for desired tilt angles of the camera. The pan motion control was achieved by designing a pan motion mechanism in the control unit to magnetically actuate the capsule. The experimental investigations indicate that our camera actuation mechanism design can achieve 0.594° and 0.524° average control errors in tilt motion control and pan motion control, respectively.

In our future work, the camera on-board electronics will be integrated especially an inertial sensor, which is used to provide the camera orientation feedback wirelessly. The dimensions and the weight of the control unit will be further reduced for convenient usage by surgeons. The control unit cables will be removed by integrating a wireless module, coil drivers, and batteries inside the control unit. The camera system will be further tested *in vivo* within a porcine abdominal cavity to verify the proposed control method and estimation methods. We will also further investigate the interference of generated magnetic field with other surgical instruments to minimize the disturbance. A proper solution for reducing the size and weight of external control unit would be replacing electromagnetic coils with permanent magnets. However, controlling the magnetic field generated solely with permanent magnets should be further investigated.

ORCID

Reza Yazdanpanah Abdolmalaki http://orcid.org/0000-0002-2540-0049

Xiaolong Liu https://orcid.org/0000-0001-5335-3473

REFERENCES

1. Desai M, Berger A, Brandina R, et al. Laparoendoscopic single-site surgery: initial hundred patients. *Urology*. 2009;74(4):805-812.
2. Saidy M, Tessier M, Tessier D. Single-incision laparoscopic surger—hype or reality: a historical control study. *Perm J*. 2012;16(1):47-50.
3. Swain P, Austin R, Bally K, Trusty R. Development and testing of a tethered, independent camera for NOTES and single-site laparoscopic procedures. *Surg Endosc*. 2010;24(8):2013-2021.
4. Cadeddu J, Fernandez R, Desai M, et al. Novel magnetically guided intra-abdominal camera to facilitate laparoendoscopic single-site surgery: initial human experience. *Surg Endosc*. 2009;23(8):1894-1899.
5. Hu T, Allen K, Hogle J, Fowler L. Insertable surgical imaging device with pan, tilt, zoom, and lighting. *Int J Rob Res*. 2009;28(10):1373-1386.
6. Terry B, Mills Z, Schoen J, Rentschler M. Single-port-access surgery with a novel magnet camera system. *IEEE Trans Biomed Eng*. 2012;59(4):1187-1193.
7. Castro C, Smith S, Alqassis A, et al. A wireless robot for networked laparoscopy. *IEEE Trans Biomed Eng*. 2013;60(4):930-936.
8. Platt S, Hawks J, Rentschler M. Vision and task assistance using modular wireless in vivo surgical robots. *IEEE Trans Biomed Eng*. 2009;56(6):1700-1710.
9. Simi M, Silvestri M, Cavallotti C, et al. Magnetically activated stereoscopic vision system for laparoendoscopic single-site surgery. *IEEE/ASME Trans Mechatron*. 2013;18(3):1140-1151.
10. Simi M, Sardi G, Valdastri P, Menciassi A, Dario P. Magnetic Levitation camera robot for endoscopic surgery. In: 2011 IEEE International Conference on Robotics and Automation (ICRA). Shanghai; 2011:5279-5284.
11. Silvestri M, Ranzani T, Argiolas A, Vatteroni M, Menciassi A. A multi-point of view 3D camera system for minimally invasive surgery. *Sensors Actuators A Phys*. 2013;202:204-210.
12. Liu X, Mancini G, Tan J. Design of a unified active locomotion mechanism for a capsule-shaped laparoscopic camera system. In: 2014 IEEE International Conference on Robotics and Automation (ICRA). Hong Kong; 2014:2449-2456.
13. Garbin N, Slawinski PR, Aiello G, Karraz C, Valdastri P. Laparoscopic camera based on an orthogonal magnet arrangement. *IEEE Robot Autom Lett*. 2016;1(2):924-929.
14. Song C, Alijani A, Frank T, Hanna G, Cuschieri A. Mechanical properties of the human abdominal wall measured in vivo during insufflation for laparoscopic surgery. *Surg Endoscopy Other Interventional Tech*. 2006;20(6):987-990.
15. Liu X, Abdolmalaki RY, Zuo T, Guan Y, Mancini GJ, Tan J. Transformable in-vivo robotic laparoscopic camera with optimized illumination system for single-port access surgery: initial prototype. *IEEE/ASME Trans Mechatron*. 2018;23(4):1585-1596.
16. Yazdanpanah AR, Liu X, Li N, Tan J. A novel laparoscopic camera robot with in-vivo lens cleaning and debris prevention modules. In: 2017 IEEE/RSJ International Conference on Intelligent Robots and Systems (IROS). Vancouver, BC; 2017:3669-3674.
17. Liu X, Mancini GJ, Guan Y, Tan J. Design of a magnetic actuated fully insertable robotic camera system for single incision laparoscopic surgery. *IEEE/ASME Trans Mechatron*. 2015;PP(99):1-1.
18. Liu X, Abdolmalaki RY, Mancini G, Tan J. Control of a magnetic actuated robotic surgical camera system for single incision laparoscopic surgery. In: 2015 IEEE International Conference on Robotics and Biomimetics (ROBIO). Zhuhai; 2015:1396-1402.